

X-ray radioscopy validation of a polyol functionalized with graphene oxide for producing rigid polyurethane foams with improved cellular structures

Mercedes Santiago-Calvo^{a,*}, Saúl Pérez-Tamarit^a, Paula Cimavilla-Román^a, Victoria Blasco^b, Carolina Ruiz^b, Rodrigo París^b, Fernando Villafañe^c, Miguel Ángel Rodríguez-Pérez^a

^a Cellular Materials Laboratory (CellMat), Condensed Matter Physics Department, Faculty of Science, University of Valladolid, Campus Miguel Delibes, Paseo de Belén 7, 47011 Valladolid, Spain

^b D.C. Technology and corporate venturing, Repsol S.A. C/ Agustín de Betancourt s/n, 28935 Móstoles, Spain

^c GIR MIOMeT-IU Cinquima-Química Inorgánica, Faculty of Science, University of Valladolid, Campus Miguel Delibes, Paseo de Belén 7, 47011 Valladolid, Spain

HIGHLIGHTS

- Polyols blends functionalized with graphene oxide (GO-f) and filled with graphene oxide particles (GO-d) are employed to produce rigid PU foams.
- The foaming behaviour of rigid polyurethane (RPU) foams with GO-f or GO-d is followed by X-Ray radioscopy.
- The cellular structure of RPU foams such as cell nucleation density and cell size are improved by incorporation of GO-f.
- GO-f offers better results than GO-d in improving the cellular structure and in providing a more reproducible process.

* Corresponding author.

E-mail address: mercesc@fmc.uva.es (Mercedes Santiago-Calvo).

X-ray radioscopy validation of a polyol functionalized with graphene oxide for producing rigid polyurethane foams with improved cellular structures

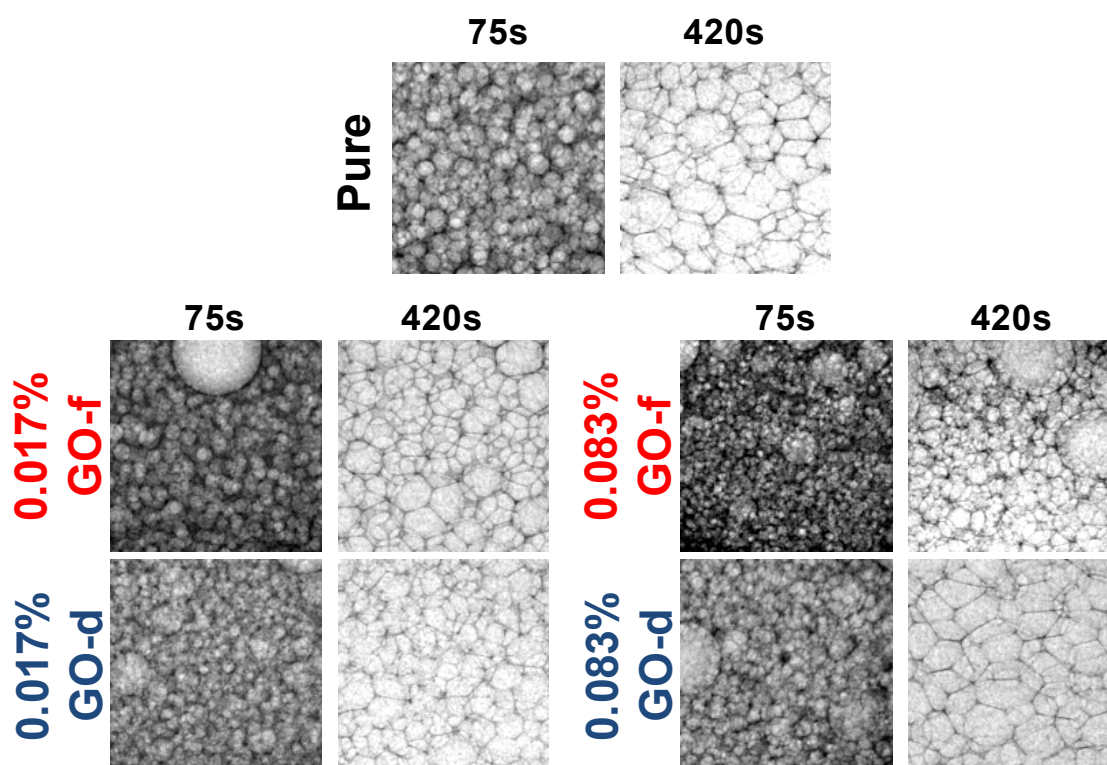
Mercedes Santiago-Calvo^{a,*}, Saúl Pérez-Tamarit^a, Paula Cimavilla-Román^a, Victoria Blasco^b, Carolina Ruiz^b, Rodrigo París^b, Fernando Villafañe^c, Miguel Ángel Rodríguez-Pérez^a

^a Cellular Materials Laboratory (CellMat), Condensed Matter Physics Department, Faculty of Science, University of Valladolid, Campus Miguel Delibes, Paseo de Belén 7, 47011 Valladolid, Spain

^b D.C. Tecnology and corporate venturing, Repsol S.A. C/ Agustín de Betancourt s/n, 28935 Móstoles, Spain

^c GIR MIOMeT-IU Cinquima-Química Inorgánica, Faculty of Science, University of Valladolid, Campus Miguel Delibes, Paseo de Belén 7, 47011 Valladolid, Spain

GRAPHICAL ABSTRACT



* Corresponding author.

E-mail address: mercesc@fmc.uva.es (Mercedes Santiago-Calvo).

X-ray radioscopy validation of a polyol functionalized with graphene oxide for producing rigid polyurethane foams with improved cellular structures

Mercedes Santiago-Calvo^{a,*}, Saúl Pérez-Tamarit^a, Paula Cimavilla-Román^a, Victoria Blasco^b, Carolina Ruiz^b, Rodrigo París, Fernando Villafañe^c, Miguel Ángel Rodríguez-Pérez^a

^a Cellular Materials Laboratory (CellMat), Condensed Matter Physics Department, Faculty of Science, University of Valladolid, Campus Miguel Delibes, Paseo de Belén 7, 47011 Valladolid, Spain

^b D.C. Technology and corporate venturing, Repsol S.A. C/ Agustín de Betancourt s/n, 28935 Móstoles, Spain

^c GIR MIOMeT-IU Cinquima-Química Inorgánica, Faculty of Science, University of Valladolid, Campus Miguel Delibes, Paseo de Belén 7, 47011 Valladolid, Spain

Keywords

Polyurethane foam; Graphene oxide; filler agglomeration; X-ray radioscopy

ABSTRACT

Fillers can be dispersed in polyurethane (PU) components to produce PU foams with improved properties by different methods. Herein, graphene oxide (GO) is chemically incorporated into the polyol chains in order to suppress fillers agglomeration. Then the foaming behaviour of rigid polyurethane (RPU) foams from polyols functionalized with GO (GO-f) are compared with RPU foams containing GO dispersed in the polyol (GO-d) by high shear mixing. Different data, such as relative density, cell size, and cell nucleation density of the RPU foam nanocomposites are monitored during the foaming process by using X-ray radioscopy. The results obtained demonstrate that the use of polyol functionalized with GO-f offers a higher degree of improvement in the cellular structure and also makes the results more reproducible.

1. Introduction

The exceptional characteristics of rigid polyurethane (RPU) foams, such as their low thermal conductivity, low density, high strength-to-weight ratio, and low moisture permeability, make them very useful materials for thermal insulation in different sectors such as transportation, refrigeration systems, automotive industry, and building construction, among others [1, 2].

* Corresponding author.

E-mail address: mercesc@fmc.uva.es (Mercedes Santiago-Calvo).

Moreover, their properties may be considerably improved by introducing fillers in the formulation. The effect of fillers on the properties of the foams depends on their concentration, their particle size and shape, their functionality, their compatibility with the polymer matrix, as well as on their degree of dispersion. The latter factor is crucial because the effect of fillers on the properties of foams is mainly correlated with an optimal dispersion into the PU matrix [3-6]. However, reaching a suitable dispersion of fillers is a complicated task. Fillers are commonly dispersed into either the isocyanate or the polyol components by using high shear mixing and/or ultrasounds [3-10], although there are also a few numbers of studies describing PU components functionalized with fillers [11-14].

In a previous study we reported the synthesis of water-blown RPU foams from polyols chemically functionalized with low amounts of graphene oxide (GO) (0.017, 0.033 and 0.083 wt%) [13], what resulted in lower cell sizes and thermal conductivities in comparison with the material without filler. Moreover, the main advantage of using GO particles chemically incorporated into the polyol chains was that agglomeration of fillers was avoided. In order to support the concept that the incorporation of GO chemically linked to polyol chains clearly improves the characteristics of RPU foams nanocomposites, we herein compare the influence of either the incorporation of GO in the polyol chains either the dispersion of GO into polyol on some of the characteristics of the foams. Relative density, cell size, and cell density of the RPU foam nanocomposites were studied by using X-ray radiography, which allows evaluating the effect of GO on the foaming mechanisms (cell nucleation and growth and degeneration mechanisms such as pore coalescence) at all intermediate stages during the foaming process.

2. Experimental

2.1. Materials

Three poly(propylene oxide) polyols synthesized by Repsol S.A. were used in this study: the pure polyol without GO (OH index 426.4 mg KOH/g, viscosity 476.9 mPa·s, 488 Dalton), and those functionalized with GO (Graphene oxide water dispersion from Graphenea S.A.): 500 ppm of GO (OH index 399.3 mg KOH/g, viscosity 553.3 mPa·s, 494 Dalton) and 2500 ppm of GO (OH index 377.5 mg KOH/g, viscosity 4463.2 mPa·s, 675 Dalton) [13].

Two series of RPU foams were studied: (1) foams synthesized with the polyols functionalized with GO (GO-f): RPU foams containing 0.017 (500 ppm of GO in polyol) and 0.083 wt% GO-f (2500 ppm of GO in polyol); and (2) foams synthesized with GO dispersed (GO-d) into the pure polyol: RPU foams containing 0.017 and 0.083 wt% GO-d. A pure material (obtained with pure polyol without GO) was used as a reference for both series.

The series of RPU foams with GO-f were synthesized following the next steps. An overhead stirrer (EUROSTAR Power control-visc P1, IKA) with a 50 mm diameter Lenart disc stirrer was used to premix a mixture of polyol synthesized by Repsol S.A [13] (100 parts by weight (ppw)), TEGOAMIN® DMCHA catalyst from Evonik (0.3 ppw), TEGOSTAB® B 8522 surfactant from Evonik (1 ppw), and distilled water as blowing agent (5 ppw). A lower amount of catalyst (0.3 ppw) is used in this study because the cream time must be increased in order to observe properly the foaming behaviour with the X-ray setup. The mixture of the components was stirred during 2 minutes at 250 rpm to obtain homogenous polyol blends (Part B). IsoPMDI 92140 (31.5% NCO, density 1.23 g cm⁻³, viscosity 170-250 mPa·s), a polymeric diphenylmethane diisocyanate (pMDI) from "BASF Poliuretanos Iberia S.A", was used. Part B and Part A were then mixed in a plastic cup at 1200 rpm for 10 seconds. The isocyanate index was fixed in 120 (Part A).

The series of RPU foams with GO-d into the pure polyol were synthesized following the same steps and the same formulation as for RPU foams with GO-f. However, a new step is necessary in this case: the production of the premix of GO with the polyol blend. For that, the GO water dispersion and the polyol blend were stirred during 5 minutes at 250 rpm for an optimal dispersion.

A total amount of 30 g (Part A and Part B) were mixed in a plastic cup, and then 0.020±0.009 ml of this reaction mixture was poured on a specific foaming mould in order to carry out the X-ray radioscapy experiments (section 2.3). In addition, the material not used in the radioscapy test was allowed to grow in the plastic cup and the resulting foam with a cylindrical size of 100 mm x 100 mm (diameter x height) was characterized (section 2.2).

2.2. Characterization of final foam

Density and mean cell size of the resulting foams obtained in a plastic cup (as mentioned in section 2.1) were measured in order to validate the X-ray radioscapy results. The values obtained were compared with those corresponding to the last monitored instant in radioscapy. Density was measured as described by ASTM D1622/D1622M-14 [15]. Relative density was obtained as the ratio between the foam density and the solid material density (1160 kg/m³). Moreover, the microstructure of the foams was examined by Scanning Electron Microscopy (SEM) with a JEOL JSM-820 microscope. Then, an image analysis protocol [16] was applied on SEM micrographs to determine the mean 3D cell size (Φ_{3D}).

2.3. X-ray Radioscapy

2.3.1. Set-up

X-ray radioscopy, in which sequences of radiographies are acquired over time, has been demonstrated to be a useful tool for the *in-situ* inspection of the foaming process of polymeric materials [17-19]. The basic elements of the radioscopy set-up used in this research are: a low energy micro-focus X-ray source which produces X-rays (L10101, Hamamatsu. Voltage: 20-100 kV, Current: 0-200 μ A), and a high sensitivity flat panel detector which forms the X-ray images (C7940DK-02, Hamamatsu. 2240x2344 pixels, 50 μ m pixel size). Both elements are positioned at a distance (source to detector distance, SDD) of 580 mm (Figure 1a). Furthermore, the magnification factor (M) is determined by the position of the monitored object between source and detector (SOD, source to object distance), considering the cone-beam provided by the X-ray source (Equation 1).

$$M = \frac{SDD}{SOD} \quad (1)$$

In this study, SOD = 46.4 mm, what leads to $M=12.5$, that resulted in an effective pixel size of 8 μ m, by using pixel binning 2x2.

2.3.2. Monitoring

A specific foaming mould (Figure 1b) was designed and fabricated using stainless steel in order to perform the X-ray radioscopy experiments. It consists on a central cylindrical hole ($\emptyset = 6$ mm, thickness = 0.6 mm) with two lateral evacuation cavities. The amount of the isocyanate-polyol mixture introduced in the central area of the mould was 0.020 ± 0.009 mL (PU droplet in Figure 1b). This blend was deposited in this area immediately after the stirring process as mentioned in section 2.1. Foaming occurred between two polypropylene plastic covers (25 μ m thick) which permitted, helped by the evacuation cavities, to maintain invariable the sample thickness during the process. Two smaller holes are located just below the centred one which enables an *in-situ* calibration of the X-ray acquired signal (Figure 1b). Two materials with known relative density (air, relative density 0 and a thermoplastic polyurethane (TPU) disc of the same thickness, relative density 1) are located in these holes and scanned with the evolving sample. The image analysis calculations in which this calibration is used are explained in the following section.

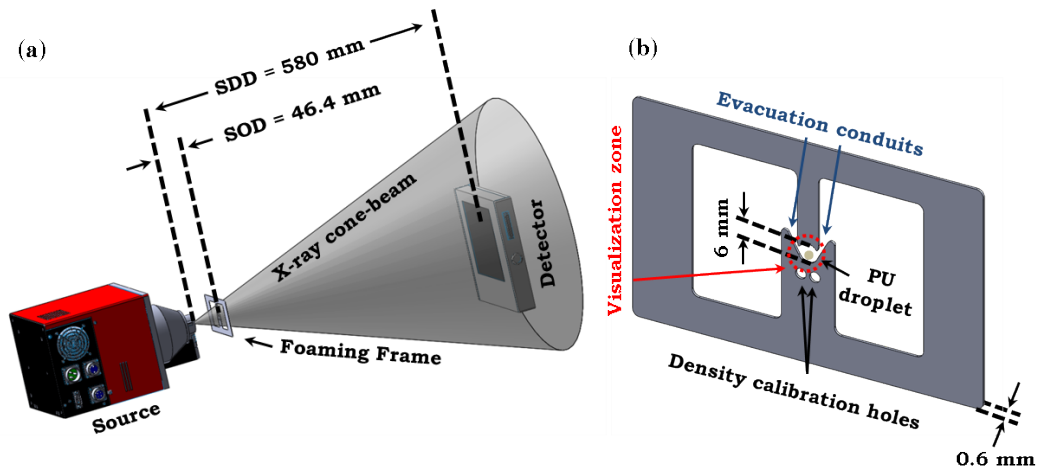


Figure 1. 3D sketch of the system employed to perform the X-ray radioscopy experiments. (a) X-ray system and relative position of the foaming mould with respect to the X-ray source and detector and (b) designed mould for PU foaming (foaming frame).

The X-ray tube was adjusted at 40 kV and 120 μ A in order to obtain the optimum contrast on the acquired radiographies. The low amount of catalyst allowed us to slow down the foaming kinetics. For this reason, an exposure time of 800 ms was selected in order to record motionless and sharp images. A total of 700 radiographies were acquired, corresponding to *ca.* 9 min of the foaming process. The first 50s are needed in order to place the foaming frame inside the X-ray cabinet. Three foaming tests were carried out for every material to obtain a representative behaviour of each formulation.

2.4. Image Analysis

Dedicated image analysis protocols have been programmed using ImageJ/Fiji as image analysis tool [20, 21]. These protocols were applied to all the acquired radiographs in order to quantify both the relative density and the cell size to finally calculate the cell density.

Density (ρ) evolution can be extracted by using the Beer-Lambert attenuation law [22], which allows calculating the density of the materials from the transmitted intensity collected in the detector (I), as expressed by Equation 2.

$$I = I_0 \exp(-\mu \rho t) \quad (2)$$

Where both the X-ray attenuation coefficient (μ) and the thickness of the sample (t) exponentially reduce the original intensity from the source (I_0). Relative density (density of the sample divided by density of the solid precursor) (ρ_r) evolution was obtained by calibrating the acquired average intensity on the sample (I) using the intensity of two materials with known

relative density. The zone used to determine the intensity on the sample has been adjusted over time to the surface occupied by the sample in the visualization zone from a little drop at the start of the process to the full 6 mm hole of the foaming frame at the end. The intensity used to determine the relative density is the average intensity in these zones over time/images. In our case, air (I_{air}) and solid TPU of 0.6 mm of thickness (I_{ref}) were located in the smaller holes of the foaming frame (Figure 1b). Zones of the same area in each of the mentioned holes have been used to calculate the average intensities of air and solid TPU respectively during the whole process. After a logarithmic conversion of the acquired intensity, relative density was calculated as the ratio between these two extreme calibration points (Equation 3 for general calibration equation and Equation 4 for our particular case with relative densities 0 and 1 as limits) [22].

$$\rho_r = \rho_r^{air} + \frac{\log\left(\frac{I}{I_{air}}\right)}{\log\left(\frac{I_{ref}}{I_{air}}\right)} (\rho_r^{ref} - \rho_r^{air}) \quad (3)$$

$$\rho_r = \frac{\log\left(\frac{I}{I_{air}}\right)}{\log\left(\frac{I_{ref}}{I_{air}}\right)} \quad (4)$$

Several sequential steps were involved in the *in-situ* determination of the cell size. Firstly, the real pixel size was scaled considering a known distance in the images. Then, an edge preserving filter allowed homogenising the intensity of the images, thus facilitating subsequent binarization. As sample intensity was exponentially decreasing (as well as relative density), the threshold limits were varied automatically being adapted to the intensity of the images, thus enabling a proper binarization of the whole sequence. After that, a watershed algorithm [23] was applied in order to separate every single pore. In order to minimise cell size quantification errors, maximum and minimum cell size at the start and at the end of the process is evaluated by the user on the images. After that, the image analysis software allowed interpolating both values for the whole sequence assuming a $t^{1/2}$ law for the cell growth, typically considered within the literature [24, 25]. As a result, maximum and minimum cell sizes are obtained during the full expansion process. In addition, only objects with circularity higher than 0.8 were included in order to refine the cell size characterization. Using both restrictions (size and circularity) we were able to avoid pore overlapping problems in addition to binarization and watershed mistakes during the image analysis process. Once the cell size is characterized on the radiographs (2D), it is transformed to 3D values using the typical scale factor of 1.27 [16].

Once cell size (ϕ) and relative density (ρ_r) were adequately monitored, the evolution of the cell nucleation density (N_o) or number of cells per unit volume of the unfoamed material was determined using Equation 5.

$$N_o = \frac{6}{\pi\phi^3} \left(\frac{1}{\rho_r} - 1 \right) \quad (5)$$

Finally, we have defined the average normalized standard deviation (Average NSD) of the three experiments performed for each sample (Equation 6). It is calculated for each parameter studied during the foaming process: relative density, cell size and cell density. Average NSD is obtained by averaging the NSD for each time of the foaming process, being NSD the ratio of the standard deviation (SD) of the parameter studied (relative density, cell size or cell density) divided by its average value for each time, once considered the three radioscapy experiments performed for the same sample.

$$\text{Average NSD} = \frac{1}{i} \sum_i \text{NSD} \quad ; \quad i = \# \text{time} \quad (6)$$

Since Average NSD is calculated from three experiments performed for each sample, this parameter accounts for the reproducibility of the experiments carried out for each material.

3. Results and discussion

3.1. Foaming behaviour

X-ray radioscapy allows following in-situ the foaming process of RPU foams. In order to compare the foams containing GO-f and those containing GO-d, three parameters have been evaluated during the foaming process: relative density, cell size, and cell density.

Figure 2 shows the evolution of the relative density during the foaming process. In general, the two series of RPU nanocomposites foam present slower expansion than the pure material at the early stages of the foaming process (60-200 s). This behaviour could be attributed to the higher viscosity of both the polyols with GO-f and the polyols with GO-d as well as to the possible chemical interaction (weak, through hydrogen bonds, or strong, through covalent bonds) between functional groups present on GO surface and the PU components.

At the end of the foaming process (ca. 560 s), the foams with GO-f reach slightly higher relative density than the reference material as the amount of GO-f increases. However, the opposite result is found for the foam with high GO-d content (0.083 wt. %), since a slightly decrease in relative density with respect to pure material is observed that the reason for this behaviour

could be related with the oxygen functional groups (epoxy, carboxyl and hydroxyl) in the GO-d surface that can form hydrogen bonds with water, and this adsorbed water is released at final stages of the foaming process producing CO₂ when it reacts with isocyanate component. For the case of GO-f, that effect is not observed maybe because part of the functional groups of their surface have reacted during the synthesis of polyol functionalized with GO and thus GO-f has less functional groups on their surface than GO-d particles which only are dispersed in the polyol.

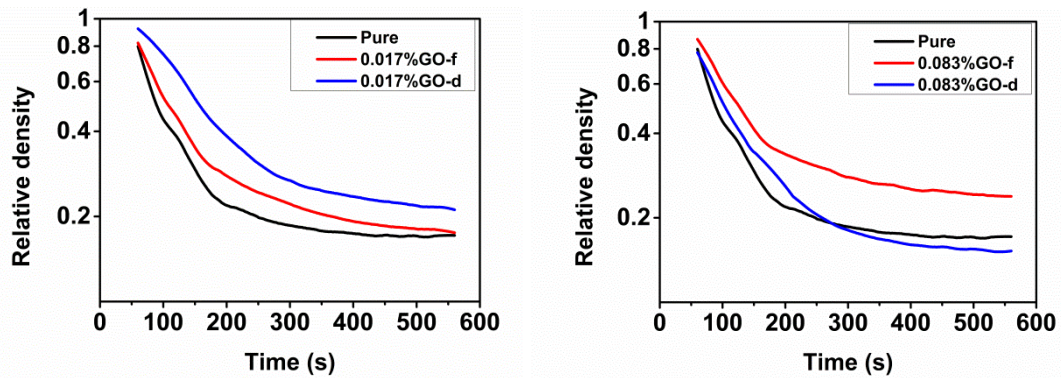


Figure 2. Evolution of relative density, measured by X-ray radioscropy, during the foaming process for the materials under study.

Figure 3 shows the values of cell size evolution, which point to a cell size reduction for both type of foams (with GO-f and with GO-d) at the beginning of PU formation. This cell size reduction is the same for low content (0.017 wt. %) of GO-f and of GO-d, whereas at high content of GO-f (0.083 wt. %) the cell size is also decreased. However, the GO-d material with a higher content of particles presents a similar cell size to that of the reference system. This result could be due to a low content of GO is dispersed easily, whereas a high content could form aggregates. In conclusion, the cell size decreases as the GO-f content increases in comparison with the reference system, being 16 % and 30% the reduction reached for 0.017 wt. % and 0.083 wt. % of GO-f, respectively. Conversely, the cell size is reduced by *ca.* 20% for foam with 0.017 wt. %, whereas the cell size is not reduced for the foam with 0.083 wt. % GO-d in comparison with the values of the reference material.

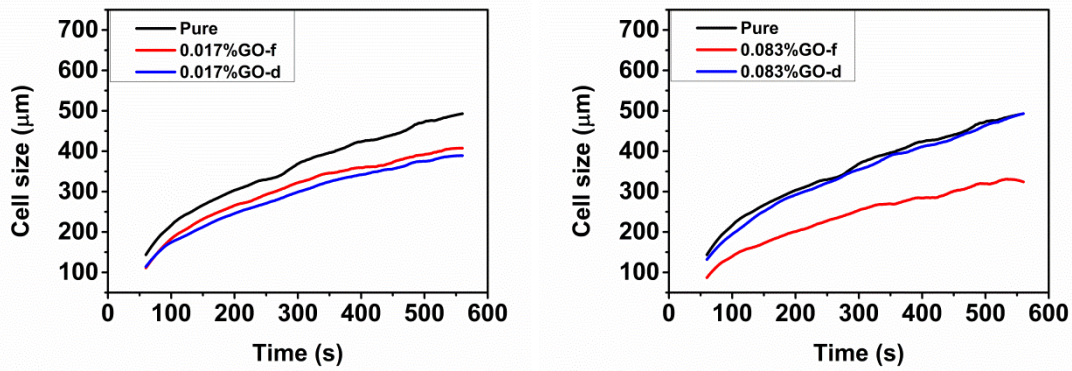


Figure 3. Evolution of the cell size , measured by X-Ray radioscopy, during the foaming process for the materials under study.

Figure 4 shows the cell nucleation density evolution during the PU formation calculated by equation 3. In all samples there is an increase of the cell nucleation density in the first instants, reaching a maximum. Then, a drop of the cell nucleation density is observed because the mechanisms of degeneration start to appear. At the early stages, the results show that the number of nucleation sites increases for the samples with GO-f compared with the reference material and those foams with GO-d, being the cell nucleation density superior for the highest GO-f content. The evolution of cell nucleation density shows that there is coalescence in all the systems under study because the cell nucleation density decreases with time, being this coalescence more pronounced in systems with GO-f. Despite this, the enhanced nucleation experienced by foams with GO-f prevails at final stages over the cell degeneration processes, which is in accordance with the cell size reduction described above.

All the above can be explained by the hydrophilic or hydrophobic character of GO particles. As mentioned earlier, the GO-d has more oxygen functional groups than GO-f, as a consequence GO-d presents more hydrophilic character while GO-f is more hydrophobic. In this way, the hydrophobic surface of GO-f favours the nucleation mechanisms due to their non-wetting surface and also causes destabilizing effects in the cell walls [19]. The opposite effect occurs in the case of foams with GO-d particles which have a more hydrophilic surface and thus it produces less destabilization of the foaming process [19]. In addition to this, the results of cell nucleation density could also relate with the improved dispersion of the particles in the system GO-f.

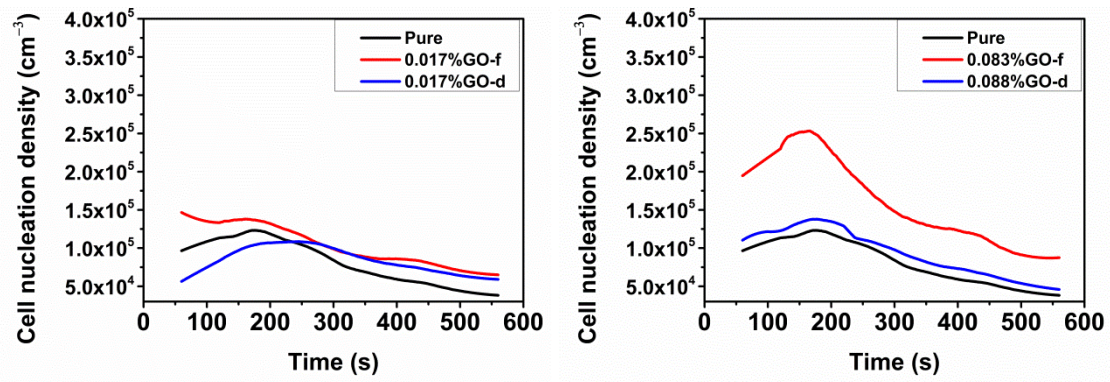


Figure 4. Evolution of the cell nucleation density, measured by X-ray radioscopy, during the foaming process for the materials.

Average NSD vales have been calculated for each parameter studied during the foaming process: relative density, cell size and cell density (Figure 5). In general, the average NSD of the systems with GO-d is higher for several of the parameters measured, followed by those with GO-f. This is clearly observed by the values of NSD for relative densities and cell nucleation densities. Hence, the reproducibility of the RPU foams with GO-d is worse than that of the foams with GO-f because the degree of GO dispersion is poorer in the GO-d system. Instead, the disadvantage of the filler dispersion is removed by using polyols functionalized with GO (GO-f).

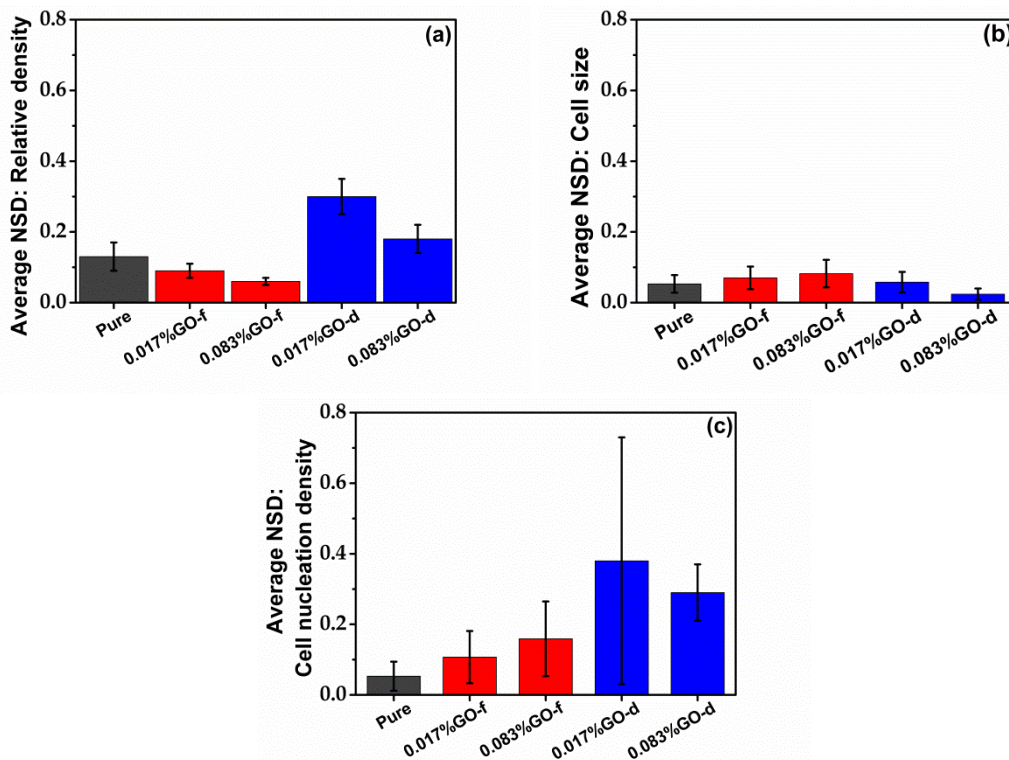


Figure 5. Average NSD for the three main parameters considered in this investigation. (a) Relative density (b) cell size and (c) cell density.

3.2. Comparison of results obtained from the radioscapy experiments and the final foam

The relative density and cell size for foams obtained with a small drop of PU mixture (0.020±0.009 ml) at 560 s of X-ray radioscapy experiment and that for final foams with a larger size (100 mm of diameter x 100 mm of height) are collected in Table 1. The foams produced during the X-ray radioscapy experiment present higher values of relative density (0.155±0.031 more) and smaller values of cell size (118±22 less) than those of the final foams. This is because these parameters are measured for smaller samples at 560 seconds when the foaming process has not yet been completed and the reduced size of the sample scanned by radioscapy limits the temperature generation and due to this its expansion. However, the trends observed in the radioscapy samples correspond to those of the larger samples which allow validating the X-ray radioscapy results. The foams containing GO-f have higher relative density than that of the reference material, whereas the foams with GO-d present a decrease in relative density with respect to the reference material. On the other hand, the average cell size decreases when increasing the amount of GO-f. The sample containing 0.017 wt. % GO-d presents similar decrease in cell size than the sample with the same content, but of GO-f, whereas the foam with 0.083 wt. % GO-d hardly reduces the cell size. Moreover, the reduction in cell size observed in the radioscapy experiments are very similar to those obtained for final materials (Table 1).

Table 1. Relative density, cell size and cell size reduction for radioscapy foams and for final foams.

Material	Radioscapy foam at 560 seconds of foaming process (smaller size)			Final foam (higher size)		
	Relative density	Cell size (µm)	Cell size reduction (%)	Relative density	Cell size (µm)	Cell size reduction (%)
Pure	0.170	489		0.0340	616	
0.017%GO-f	0.178	413	16	0.0381	524	15
0.083%GO-f	0.239	341	30	0.0404	476	23
0.017%GO-d	0.210	390	20	0.0339	523	15
0.083%GO-d	0.151	502	0	0.0249	585	5

4. Conclusions

Relative density, cell size and cell nucleation density have been measured during the foaming process of rigid PU foams containing GO nanoparticles. These particles have been introduced by two different methods: by using polyols functionalized with GO and by dispersing the particles into the polyol using high shear mixing.

The radioscopy results have shown that the addition of the particles improves the nucleation process, reducing the cell sizes in the early stages of the foaming process. For the systems containing GO-f particles this improvement is progressive, i.e. a higher amount of particles results in better improvements. A superior cell nucleation density and a cell size decrease of 30% for the highest GO-f content of 0.083 wt% has been achieved. However, for the systems containing GO-d particles, the improvement almost disappears when a high amount of particles is added (0.083 w% GO-d) because it is most difficult to achieve a proper dispersion of the fillers when the amount increases. Furthermore, the systems with GO-d present higher average NSD of the relative density and cell nucleation density than that of the systems with GO-f. Therefore, the reproducibility of the experiments is better for the foams obtained with GO-f mainly because the dispersion is improved in these materials.

Acknowledgements

Financial assistance from MINECO, FEDER, UE (MAT2015-69234-R) and the Junta de Castile and Leon (VA275P18) are gratefully acknowledged. Authors thank Graphenea S.A. for supplying us with Graphene Oxide and for the technical discussion. Predoctoral contract of S. Perez-Tamarit by University of Valladolid (E-47-2015-0094701) and co-financed by Banco Santander is also acknowledged. Financial support from Junta de Castilla y Leon predoctoral grant of P. Cimavilla-Román, co-financed by the European Social Fund is also acknowledged.

Data Availability

The raw/processed data required to reproduce these findings cannot be shared at this time as the data also forms part of an ongoing study.

References

- [1] M. Szycher, Szycher's Handbook of Polyurethanes, Second ed., CRC Press Boca Raton, Florida, USA, 2012.
- [2] C. Hopmann, R. Wagner, K. Fischer, A. Böttcher, One Step Production of Highperformance Sandwich Components, Cellular Polymers, 36 (2017).

- [3] G. Harikrishnan, S.N. Singh, E. Kiesel, C.W. Macosko, Nanodispersions of carbon nanofiber for polyurethane foaming, *Polymer*, 51 (2010) 3349-3353.
- [4] M.C. Saha, M.E. Kabir, S. Jeelani, Enhancement in thermal and mechanical properties of polyurethane foam infused with nanoparticles, *Materials Science and Engineering: A*, 479 (2008) 213-222.
- [5] S. Estravís, J. Tirado-Mediavilla, M. Santiago-Calvo, J.L. Ruiz-Herrero, F. Villafañe, M.A. Rodríguez-Pérez, Rigid polyurethane foams with infused nanoclays: Relationship between cellular structure and thermal conductivity, *European Polymer Journal*, 80 (2016) 1-15.
- [6] M.E. Kabir, M.C. Saha, S. Jeelani, Effect of ultrasound sonication in carbon nanofibers/polyurethane foam composite, *Materials Science and Engineering: A*, 459 (2007) 111-116.
- [7] M. Santiago-Calvo, J. Tirado-Mediavilla, J.L. Ruiz-Herrero, M.Á. Rodríguez-Pérez, F. Villafañe, The effects of functional nanofillers on the reaction kinetics, microstructure, thermal and mechanical properties of water blown rigid polyurethane foams, *Polymer*, 150 (2018) 138-149.
- [8] S.H. Kim, M.C. Lee, H.D. Kim, H.C. Park, H.M. Jeong, K.S. Yoon, B.K. Kim, Nanoclay reinforced rigid polyurethane foams, *Journal of Applied Polymer Science*, 117 (2010) 1992-1997.
- [9] M.M.A. Nikje, Z.M. Tehrani, Thermal and mechanical properties of polyurethane rigid foam/modified nanosilica composite, *Polymer Engineering & Science*, 50 (2010) 468-473.
- [10] L. Zhang, E.D. Yilmaz, J. Schjødt-Thomsen, J.C. Rauhe, R. Pyrz, MWNT reinforced polyurethane foam: Processing, characterization and modelling of mechanical properties, *Composites Science and Technology*, 71 (2011) 877-884.
- [11] M.C. Lopes, H. Ribeiro, M.C.G.a. Santos, L.M. Seara, F.L.Q. Ferreira, R.L. Lavall, G.G. Silva, High performance polyurethane composites with isocyanate-functionalized carbon nanotubes: Improvements in tear strength and scratch hardness, *Journal of applied polymer science*, 134 (2017) 1-13.
- [12] S.M. Kang, M.J. Kim, S.H. Kwon, H. Park, H.M. Jeong, B.K. Kim, Polyurethane foam/silica chemical hybrids for shape memory effects, *Journal of Materials Research*, 27 (2012) 2837-2843.
- [13] M. Santiago-Calvo, V. Blasco, C. Ruiz, R. París, F. Villafañe, M.Á. Rodríguez-Pérez, Synthesis, characterization and physical properties of rigid polyurethane foams prepared with poly(propylene oxide) polyols containing graphene oxide, *European Polymer Journal*, 97 (2017) 230-240.
- [14] A.-K. Appel, R. Thomann, R. Mülhaupt, Hydroxyalkylation and Polyether Polyol Grafting of Graphene Tailored for Graphene/Polyurethane Nanocomposites, *Macromolecular Rapid Communications*, 34 (2013) 1249-1255.
- [15] ASTM D1622-08: Standard Test Method for Apparent Density of Rigid Cellular Plastics.
- [16] J. Pinto, E. Solorzano, M.A. Rodriguez-Perez, J.A. de Saja, Characterization of the cellular structure based on user-interactive image analysis procedures, *Journal of Cellular Plastics*, 49 (2013) 555-575.
- [17] S. Pardo-Alonso, E. Solórzano, S. Estravís, M.A. Rodríguez-Perez, J.A. de Saja, In situ evidence of the nanoparticle nucleating effect in polyurethane-nanoclay foamed systems, *Soft Matter*, 8 (2012) 11262.
- [18] S. Pardo-Alonso, E. Solórzano, M.A. Rodriguez-Perez, Time-resolved X-ray imaging of nanofiller-polyurethane reactive foam systems, *Colloids and Surfaces A: Physicochemical and Engineering Aspects*, 438 (2013) 119-125.
- [19] M. Mar Bernal, S. Pardo-Alonso, E. Solórzano, M.Á. Lopez-Manchado, R. Verdejo, M.Á. Rodríguez-Perez, Effect of carbon nanofillers on flexible polyurethane foaming from a chemical and physical perspective, *RSC Advances*, 4 (2014) 20761.
- [20] M.D. Abràmoff, P.J. Magalhães, S.J. Ram, Image Processing with ImageJ, *Biophotonics International*, 11 (2004) 36-42.

- [21] C.A. Schneider, W.S. Rasband, K.W. Eliceiri, NIH Image to ImageJ: 25 years of image analysis, *Nature Methods*, 9 (2012) 671-675.
- [22] E. Solórzano, J. Pinto, S. Pardo, F. Garcia-Moreno, M.A. Rodriguez-Perez, Application of a microfocus X-ray imaging apparatus to the study of cellular polymers, *Polymer Testing*, 32 (2013) 321-329.
- [23] L. Vincent, P. Soille, Watersheds in digital spaces: an efficient algorithm based on immersion simulations, *IEEE Transactions on Pattern Analysis and Machine Intelligence*, 13 (1991) 583 - 598.
- [24] M. Amon, C.D. Denson, A study of the dynamics of foam growth: Analysis of the growth of closely spaced spherical bubbles, *Polymer Engineering & Science*, 24 (1984) 1026-1034.
- [25] R. D.Patel, Bubble growth in a viscous Newtonian liquid, *Chemical Engineering Science*, 35 (1980) 2352-2356.